Study by transmission electron microscopy of Co-WC/Ni interface produced by solid state bonding

J. Lemus-Ruiz and G. Castro-Sánchez

Instituto de Investigación en Metalurgia y Materiales, Universidad Michoacana de San Nicolás de Hidalgo, Edificio U, Av. Francisco J. Múgica s/n, Ciudad Universitaria, Morelia 58030, Morelia, Michoacán México.
e-mail: jlruiz@umich.mx; gustavo yx@hotmail.com

J. Reyes-Gasga and R. García-García

Instituto de Física, Universidad Nacional Autónoma de México,
Circuito de la Investigación Científica s/n. Cd. Universitaria, 04510 Coyoacán, Ciudad de México, México.
e-mail: jreyes@fisica.unam.mx; ramiro@fisica.unam.mx

J. L. Marulanda-Arevalo

Facultad de Ingeniería Mecánica, Universidad Tecnológica de Pereira, Grupo de Investigación en Materiales Avanzados, Cerrada 27 No. 10-02, Los Álamos, Pereira-Risalda, Colombia,
e-mail: jlmarulanda@utp.edu.co

L. Ortega-Cabello

Departamento de Sistemas Biológicos, Universidad Autónoma Metropolitana-Xochimilco, Calzada del Hueso 1100, Colonia Villa Quietud, 04960 Coyoacán, Ciudad de México, México.
e-mail: orcalu.qfb@gmail.com

Received 27 April 2023; accepted 1 April 2024

The microstructure of the interface and inter-diffusion behavior during bonding plays an important role to understand and to control the joining process for better mechanical properties of an interface. In this work, the microstructure of the formed interlayer between cermet WC-Co and metallic Ni after solid state bonding (the WC-Co/Ni interface) was analyzed by scanning (SEM) and transmission (TEM) electron microscopy, and characteristic energy dispersive x-ray spectroscopy (EDS). The WC-Co/Ni joint was produced at 980°C for 25 minutes in argon atmosphere. For SEM observation, the samples were mechanically polished and etched. TEM samples were produced parallel (sample P), perpendicular (sample T) and oblique (sample TP) to the interface by focused ion beam (FIB). The EDS results indicate the inter-diffusion at the interface of W, Ni, Co and C and the segregation of Ni and Co, together with the formation of crystalline phases and an amorphous carbon layer. W follows a homogeneous diffusion while Ni and Co show a non-homogeneous diffusion behavior.

Keywords: WC-Co/Ni interface; solid state bonding; diffusion; characteristic energy-dispersive x-ray spectroscopy; electron microscopy.

DOI: https://doi.org/10.31349/RevMexFis.70.051601

1. Introduction

Bonding of a ceramic with a metal makes possible the combination of the ceramic hardness and the metal toughness to increase wear resistance, mainly at high temperatures. However, their joint presents some problems since the mechanical properties depend on the wettability of the ceramic by the metal, the difference in the thermal expansion coefficients, the deformation of the metal, and the eventual formation of fragile phases at the interface. All this may cause the development of tensions at the interface that could result in a premature failure of the joint. Many studies have been done to understand and improve the properties of these joints. Ceja-Cárdenas *et al*. [1] observed, for example, the formation of different Nb-silicides during joining of Si3N4 by liquid state bonding using Nb-foil interlayer and Cu-Zn foil as joining elements. Barrena *et al*. [2] reported the quality of diffusion bonding interfaces formed by cemented carbide (WC-15Co) and a cold work tool steel (90MnCrV8). They indicated that the tensile strength registered confirms the metal/ceramic bonding as a very promising technology for industrial applications, but studies on fragility sources should be done. Hosseini *et al*. [3] attributed a poor cracking resistance to the joints produced with Inconel 617 and 310 stainless steel in a wide range of solidification temperatures. In this case, they indicated the presence of low melting point secondary phases. Martinsen *et al*. [4] indicated that the production of metal/ceramic ensembles with high mechanical resistance in bonding of dissimilar materials is difficult, but a good alternative is the joining by solid state diffusion. In the bonding by diffusion, a monolithic joint is obtained by atomic bonds thanks to the diffusion of atoms from one crystal lattice side to the other to eliminate differences in concentration. Homogeneous joints are produced depending on the activation energy. Uzkut *et al*. [5] observed in SAE1040-WC materials joined by brazing that the activation energy comes from the thermal vibrations, and, if there are vacancies or other crystalline defects in the lattice, the atoms move from sites

of high to low concentration. Alternatively, Sayman *et al.* [6] calculated the thermal stress during the cooling process from 1000°C to room temperature in WC-Co/Cr-Ni multilayer coating deposited on 316L steel. They indicated that the compressive and tensile stresses occurred due to the difference in thermal expansion coefficients in each material. The tungsten carbide (WC) is an advanced ceramic very attractive for anti-wear applications in, for example, metal cutting tools, mining and agricultural machinery among others. The cermet cobalt-tungsten carbide (WC-Co) consists of WC particles embedded in Co binder. Lemus-Ruiz *et al.* [7] observed a diffusion zone at the WC/Ni interface and pointed out that the joining of these materials occurs by diffusion in solid state. They found out a strong relationship between the mechanical properties of the joint and the diffusion zone thickness. In regard to the surface roughness of the pieces to be joined, Guo *et al.* [8] observed a rapidly diffusion bonded of WC-Co to 40Cr steel with pure Ni interlayers using plasma activated sintering at 750°C and a pressure of 40 MPa. They indicated that the shear strength increased when surface roughness decrease. On the other hand, Bonny *et al.* [9] studied the wear properties of WC-Co and observed wear differences in more than one order of magnitude depending on the Co concentration. A better understanding of the bonding mechanism between carbides and metals would allow the combination of their properties. Poniznik *et al.* [10] showed that interactions such as resistance to temperature, pressure and mechanical load, to produce for example electronic devices, medical equipment and transport, depend on the properties developed at the interface, on the material porosity, and on the defects within the metal. Feng *et al.* [11] indicated that a WC-Co/Ni composite has been successfully used to join the cermet WC-Co with steel. Chen *et al.* [12] indicated that the transition layer observed between Ni and WC-Co layers helps to relax thermal stress. In this work, the WC-Co/Ni interface produced by solid-phase diffusion is analyzed by scanning (SEM) and transmission (TEM) electron microscopy, and energy-dispersive x-rays spectroscopy (EDS). The surface roughness of the materilas before joining was measured by the atomic force microscope (AFM). At the light of correlation interaction of the components, the behavior W, C, Co and Ni concentrations as function of the distance of penetration by diffusion is commented.

2. Experimental setup and methodology

Cylindrical specimens of commercial grade cermet (WC with 6% Co, Goodfellow, England) and nickel (Ni-99.5%) with 0.125 inches long and 0.25 inch in diameter were used. To obtain joint faces as flat as possible, the surfaces were initially devastated with a diamond grain disc, and sanded with silicon carbide grinding paper (SiC) from 600 to 1000 grit numbers. The surfaces were polished using 1 μm diamond paste and 0.3 μm to 0.05 μm alumina suspensions. Before bonding, the samples were cleaned with isopropanol in and ultrasonic bath for 5 minutes.

2.1. Joining experiments

The solid phase diffusion bonding of WC-6%Co with Ni was performed by axially mounting the assembly with the polished surfaces in contact in a graphite die. The assembly was placed in a screw and pressuring turning clockwise, adjusting the movement to always maintain the contact of the surfaces during bonding. A boron nitride bed (99.5%) was set around the assembly to eliminate contact and reaction between the samples and the graphite walls. The die was placed in a horizontal resistance furnace chamber inside a 30 inch in length and 3 inch in diameter alumina tube. Bonding was performed at 980°C in an argon atmosphere for 25 minutes. This temperature is much lower than the melting point of Ni (1453°C approximately). To avoid macroscopic deformations of nickel, the applied force was a fraction of the creep stress at the bonding temperature. In addition, the pressure eliminates any possible oxide layer in the contact surfaces, resulting in a better bond of the materials.

2.2. SEM sample preparation and EDS analysis

The obtained WC-Co/Ni joint was sliced with an ISOMET 1000 low-speed precision cutter to obtain the cross section of the interface. The sample was grinded with 120 to 4000 grit SiC emery paper and polished with 5 to 0.05 microns' alumina powder. Figures 1a) and 1b) show the backscattering (BSE) SEM images of the interface after polishing to mirror finish. Note the micrometric step produced at interface in the WC-Co side by the difference in grinding: Ni grinds faster than WC-Co [Fig. 1b)]. This step plays an important role in the structural analysis of the interface by electron microscopy and, therefore, its orientation relative to the direction of the incident electron beam must be known in detail. Figure 2a) indicates the case where the plane of the interface is parallel to the direction of the incident beam, and the interface is well observed. When the plane of the interface is tilted clockwise [Fig. 2b)], the interface is fully exposed to the incident electron beam, whereas when it is tilted counterclockwise [Fig. 2c)], the WC-Co step partially covers the

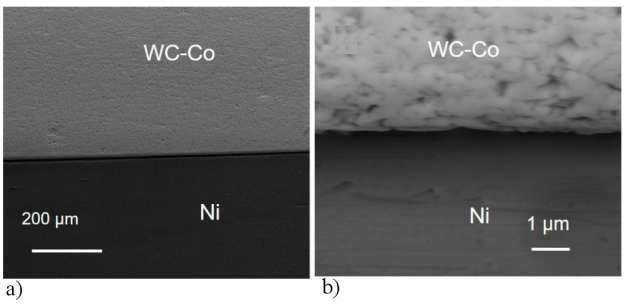

FIGURE 1. a) BSE-SEM image of 6Co-WC/Ni interface. b) Higher magnification of the image shown in a). Note the contrast presented at the interface.

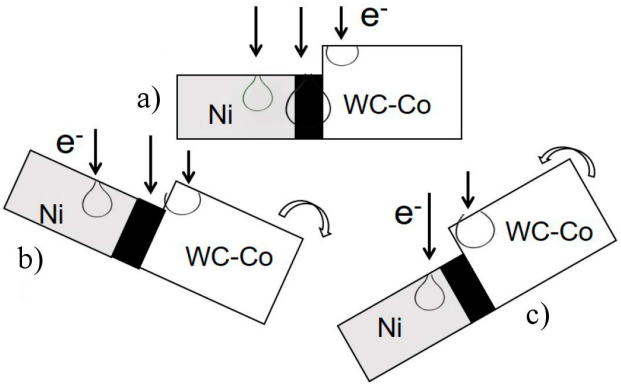

FIGURE 2. Schematic representation of the micrometric step produced at the interface. The interface plane a) parallel, b) tilted clockwise and c) tilted counterclockwise to the incident electron beam direction. The volume of interaction is also included.

interface. In addition, the WC-Co step will produce the edge effect, mainly in the secondary (SE) SEM images.

The samples were analyzed by EDS around the interface both in the point and in the line-scan modes during 180 seconds. A SEM Jeol JSM-7800F (JEOL, Tokyo, Japan) with a field emission filament and an Oxford-EDS analyzer model X-MAX (Oxford Instruments, Oxfordshire, UK) with AZtec 2.2 software were used. To determine the correlation between the number of counts per second (cps) obtained with the electron affinity, the oxidation number, the atomic radius ionization energy, and the electronegativity of the elements, the JMP computer package® version 13 was used.

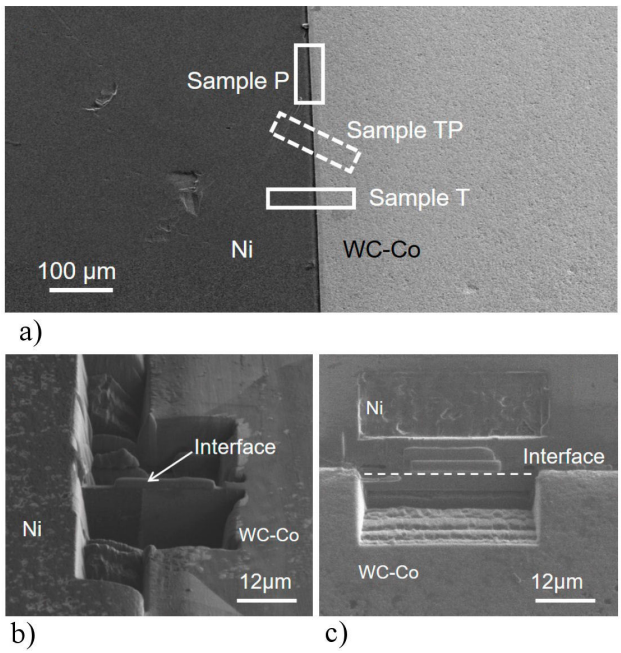

FIGURE 3. a) BSE-SEM image in cross-section of the interface indicating the sites of the FIB cuts to obtain the parallel (Sample P), transverse (Sample T) and oblique (Sample TP) samples. SE-SEM images of the b) T and c) P sample cuts.

2.3. TEM sample preparation

TEM samples were prepared with the focus ion beam (FIB) equipment FIB-FEI QUANTA 200-3D (Thermo Fisher Scientific, Hillsboro, Oregon, USA) equipped with a field emission electron gun and a gallium ion source. The TEM cross-cuts samples were made with Ga-ion beam while the sample was observed by SEM throughout the cutting. Acceleration voltage was up to 30 kV for the two beams at probe currents of 200 nA for the electron beam and 50 nA for the ion beam. The micromanipulator OmniprobeTM 100.7 equipped with gas injection systems for deposition of Platinum was used for in situ lifting of the TEM samples. Low-acceleration voltage beam was used as final polishing stage for damage reduction. Samples were cut parallel (Sample P), transverse (Sample T) and oblique (Sample TP) to the interface. Figure 3a) shows a cross-section BSE-SEM image of the interface indicating the site from where the samples were obtained. Figures 3b) and 3c) show the SE-SEM images of the cut-off made to obtain the T and P samples, respectively. A Titan-300 FEI microscope (Thermo Fisher Scientific, Hillsboro, Oregon, USA) equipped with a field emission filament operated at 300 KV and a double-tilt-sample TEM holder were used.

3. Results and discussion

WC-Co and Ni components of the interface were single phases. X-ray diffraction indicated that WC-6Co has a hexagonal unit cell with lattice parameters $a = 0.290$ nm and $c = 0.284$ and space group P6m2 (PDF card No. 03-065-8828), and Ni has a FCC unit cell with lattice parameters $a = 0.352$ nm and space group Fm3m (PDF card No. 03-065-2865).

3.1. SEM and EDS results

As it is well known, the SE-SEM images show the morphology of the sample's surface, while the BSE-SEM images are related to its atomic number Z. Because Z is 74 for W, 28 for Ni, 27 for Co and 6 for C, the BSE-SEM contrast for W is bright, for Ni is dark gray and for Co is light gray, and or C is black. EDS spectra indicated that the concentration value of the elements is a function of the distance to the interface plane: more variation is observed closer to the interface (around 3 μm, approximately). Table I shows the W, C, Co and Ni concentration values (in wt%) of 6 EDS spectra taken around the interface, together with the mean and the standard deviation of these values. Note the interdiffusion of Ni in WC-Co and C, Co, and W, in Ni at the interface.

Figure 4 shows an 18 μm in length BSE-SEM image of the interface in cross-section together with the line along which the Ni_{K_α}, W_{L_α}, C_{K_α}, and Co_{K_α} EDS line-scans were obtained. Note that the EDS line-scans occur in the range of 0 to 4000 cps for Ni, of 0 to 1200 cps for W, of 0 to 300 cps for Co, of 0 to 60 cps for C, and of 0 to 10 for O at the same

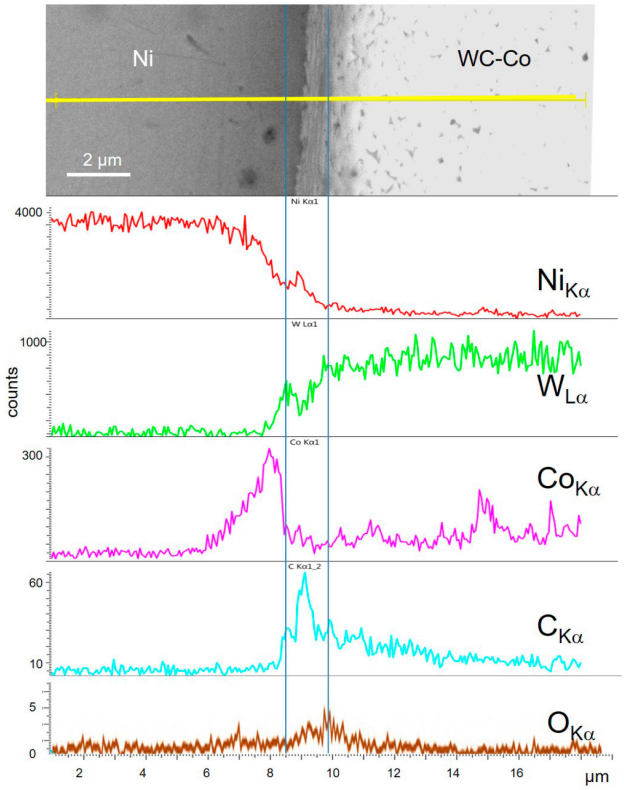

FIGURE 4. A 18 μm in length BSE-SEM image of the interface shown in Fig. 1c) and the line along which the EDS line-scans of Ni, W, Co, C, and O were obtained.

period of time (180 s). Note the peaks observed in the line scans around the interface and a interdiffusion layer of 0.5 μm, approximately. Figure 4 compares in detail the EDS line-scans of Ni and Co with that of W, and show the existence of a diffusion layer of around 0.25 to 0.50 μm. It is worth mentioning that in the case of the oxygen content, its concentration recorded by EDS in this system is very small (the O concentration recorded was 1.36 ± 0.21 wt% which practically falls within the noise of the EDS spectrum. Then Fig. 4 indicates the displacement of Co and W towards the Ni side and of Ni towards the WC-Co side. Similar Co segregation was also observed by Avettand-Fénoël *et al.* [13]. This indicates that the interface is an area where WC-Co and Ni combine and where new phases are located. Note in Fig. 4 the peaks presented by the Co and Ni lines close the interface. There is a notorious zone of 3 microns in length approximately where the Co concentration in Ni is relatively high. This indicates the possible formation of a Co based solution oversaturated in Ni. An important component for the analysis of the interface is the transition layer formed by the interdiffusion of W, Co and Ni [14]. Zhang *et al.* [15] reported that some properties of materials are influenced or controlled by the presence of this layer. Markworth *et al.* [16] reported that the transition layer could be a buffer zone for thermal expansion because thermal stresses can be relaxed in there by gradually varying the microstructure, compositions, and properties.

When comparing the EDS line-scan of Ni and Co with that of W the diffusion layer is of 0.25 to 0.50 μm wide, approximately. Unlike Chen *et al.*[12], where a continuous decreasing of the W and Ni line scans were registered, in here there are peaks in the Ni and Co concentrations. The multivariate analysis done with the JMp Computer Package and shown in Fig. 5a) explains 95% of the variability of the EDS data shown in Table 1, and finds the correlation between the elements involved.

Figure 5b) indicates that the number of counts in the EDS spectra has, as expected, a direct correlation with electronic affinity and an inverse correlation with ionization energy (correlation coefficient of 0.7604 and -0.7586 respectively). No correlation was found with oxidation number, atomic radius and electronegativity. This indicates why Ni shows a gradual decrease with Co. As it can be seen in Fig. 5a), this result is compatible with the correlation coefficient of the electronic affinity and the ionization energy decrease (0.5723 and -0.5521 respectively). It is worth to say that, although amorphous carbon was formed at low temperatures, when the formation of this interface occurs during the

TABLE I. EDS values in wt% of the elements in the Ni and WC-Co zones from 6 spectra taken around the interface.

				Part WC-Co				
Element	Nominal composition	Spectrum 1	Spectrum 2	Spectrum 3	Spectrum 4	Spectrum 5	Spectrum 6	Mean $\pm$ SD
W	85.95	78.06	50.54	83.19	86.38	81.38	87.39	77.80 ± 13.79
C	9.55	8.34	7.14	11.39	9.58	17.19	10.26	10.66 ± 3.56
Co	4.50	2.23	8.92	4.35	2.49	0.93	1.89	3.47 ± 2.90
Ni	0	11.37	33.40	1.07	1.56	0.49	0.46	8.06 ± 13.11
				Part Ni				
W	0	3.06	4.67	4.97	0.48	0.45	0.29	2.32 ± 2.20
C	0	3.57	19.88	19.88	5.79	4.64	4.80	9.26 ± 7.16
Co	0	10.53	1.21	1.21	0.58	0.13	1.61	2.65 ± 3.91
Ni	100	82.50	74.24	74.34	93.15	94.77	93.30	85.38 ± 9.65

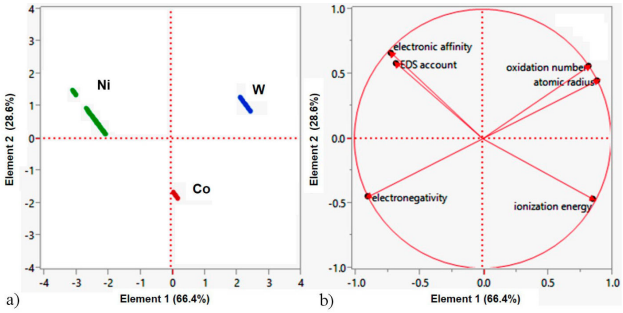

FIGURE 5. Correlation analysis of the main elements at the interface. a) Positioning of Ni, W, and Co in the correlation graph. b) Positioning of the electronic affinity, oxidation number, atomic radius, electronegativity and ionization energy in the correlation sample according with the EDS spectra.

reaction, the carbon content decreases, which means that, due to the presence of tungsten and nickel, carbon cannot be considered for this correlation analysis.

3.2. TEM analysis results

Figure 6 shows the TEM image of the sample parallel to the interface (Sample P), and the EDS spectrum and the selected area electron diffraction (SAED) pattern of zone 1 indicates that its main component is amorphous carbon [17]. The EDS spectrum the SAED pattern of zone 2 indicate a Ni polycrystalline zone. Then the cutting-off of sample P was in such a way that a piece of the Ni side was included.

Regarding the carbon area, the experimental procedure carried out was in non-equilibrium and this could cause the WC decomposition. The use of an atmosphere with low oxygen potential could also produce the ceramic decomposition at lower temperatures. As indicated in the experimental description, a boron nitride bed was set around the assembly to eliminate contact and the reaction between sample with the graphite walls. Therefore, it is highly probable that the amorphous carbon layer at the WC-Co/Ni interface was produced during the joining process by the carbon diffusion from WC-Co to Ni, so reducing system energy and the carbon content in the WC-Co layer. An interesting fact is the not observation of the carbon layer by SEM when immersed in the Ni-WC-

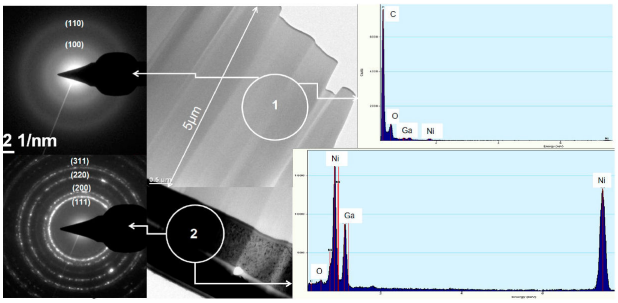

FIGURE 6. TEM image of sample P. The circles indicate the areas from which the SAED patterns (on the left) and the EDS spectra (on the right) were obtained. Zone 1 corresponds to amorphous carbon. Zone 2 corresponds to polycrystalline Ni.

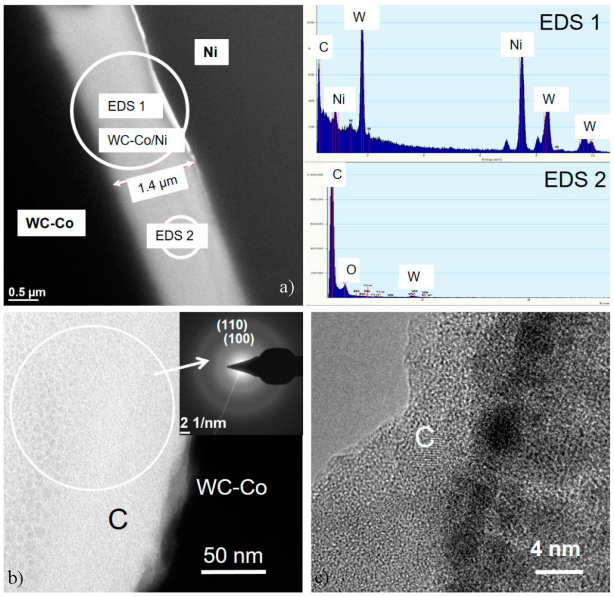

FIGURE 7. a) TEM image of sample T. The EDS 1 spectrum includes both sides of the interface. The EDS 2 spectrum and the SAED pattern shown in the insert indicate that the bright zone corresponds to an amorphous carbon layer. b) Bright field TEM image at the WC-Co side. c) HRTEM image of the carbon layer.

Co system. In the case of SE-SEM images, since they present the surface morphology, the lack of contrast of the carbon layer is straight. But this is not in the case for the BSE-SEM images, since the contrast is related to the atomic number Z of the samples material. As commented above, the contrast of W must be bright, Ni appears in dark gray, Co in light gray, and C in black. Here, the sample preparation has something to do with the not-observation of the C layer, and the orientation relationship of the interface plane with the incident beam direction play an important role. In the contrast of the SE-SEM image, the increase in intensity due to the edge effect of the WC step can hide the C layer. In the contrast of BSE-SEM image, the C layer should appear dark, but the interaction volume, which for C it is a few microns in size, includes both W and Ni, and this could reduce visibility of the C layer. It is also important to note that, in the same period of time, the EDS line-scan spectrum of Ni is in the range of 0 to 4000 cps, while for W its occurs from 0 to 1200 cps, for Co it is in the range of 0 to 300 cps, and for C the EDS spectrum is in the range of 0 to 60 cps. All this together could produce that the C layer is not observed in the BSE-SEM image although the EDS spectra do present the C signal.

Figure 7 shows the TEM image of the sample perpendicular to the interface (sample T), which contains both the Ni and WC-Co sides. The EDS spectrum labeled as 2 and the SAED pattern also indicate that the bright zone corresponds to an amorphous carbon layer of 1.4 μm in thickness. EDS spectrum 1 shows the Ni, W and C peaks because the analyzed area includes both sides of the interface. A bright field TEM image and a HRTEM image of the carbon layer are shown in Figs. 7b) and 7c), respectively. The nanometric

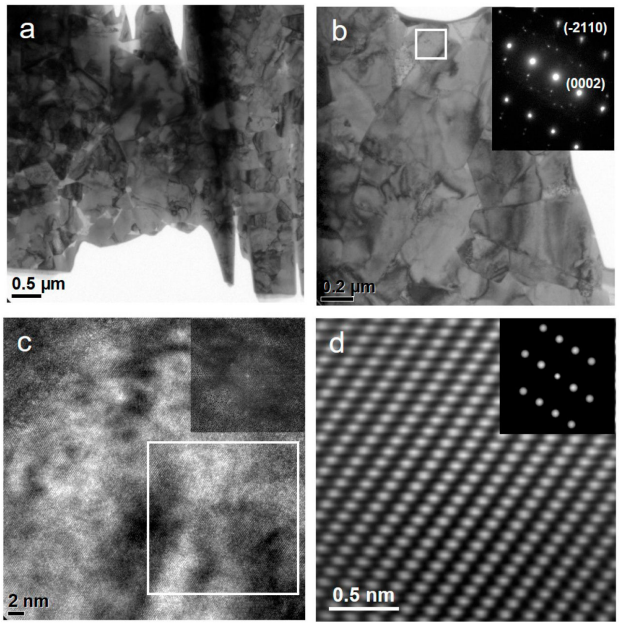

FIGURE 8. TEM images of sample T at the WC-Co side. a)-b) Bright field images. The insert in b) shows the SAED pattern along the [10-10] zone axis from the squared area. c) HRTEM image of the squared area in b). The insert shows the FFT of the squared area. d) Processed image of the squared area in c). The insert shows the filter used for processing.

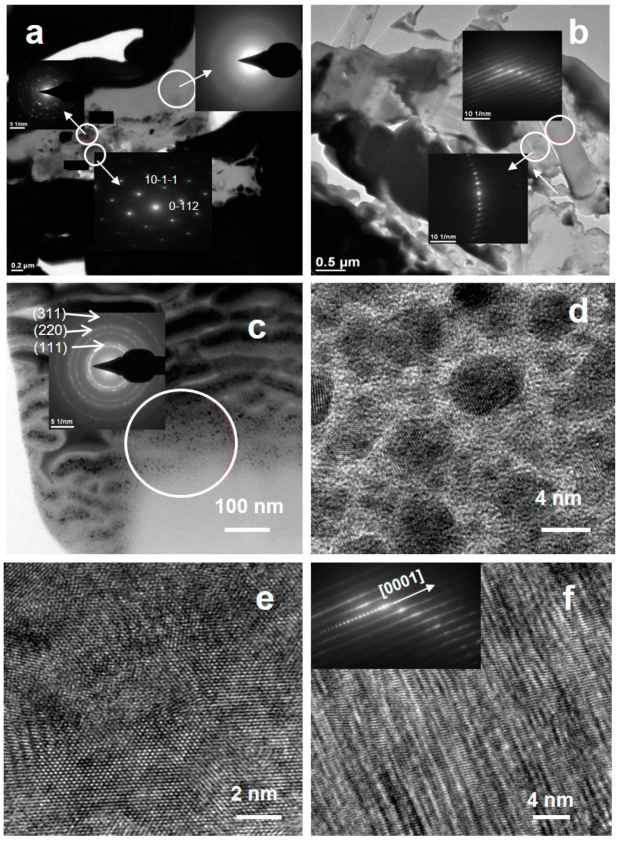

FIGURE 9. a)-c) TEM images of sample TP. The circles show the sites from where the SAED patterns were obtained. Amorphous carbon, crystalline phases and nanoparticles are observed. The SAED pattern indicates that these are Ni nanoparticles. d) HRTEM image of the nanoparticles. e) HRTEM image of a polycrystalline zone. f) HRTEM from (b). The SAED pattern indicates the presence of structural disorder along the c axis of the WC unit cell.

particles in the carbon layer could be produced by the interaction of the electron beam with carbon layer; *i.e.* they could be a product of electron radiation damage in TEM [18-21]. Once the sample T was further thinned, TEM images of the Ni and cermet WC-Co zones were better observed. Figure 8 shows the TEM images of the WC-Co side. The bright field images [(Figs. 8a) and 8b)] indicated an average grain size for the cermet of 0.5 μm, approximately, while in Ni it is of 5 μm. The SAED pattern in the insert of Fig. 8b) corresponds to the [10-10] zone axis of the WC-Co unit cell. Figure 8c shows the HRTEM image of WC-Co and Fig. 8d) shows the processed image of this last image. The contrast shown in Fig. 8c) is produced by dislocations in the Ni grains [13]. Figure 9 shows the TEM images and SAED patterns of sample TP, oblique to the interface, where the amorphous carbon, nanoparticles and crystalline zones are seen. The nanoparticles were identified as Ni (these Ni nanoparticles could be produced by the FIB Ga-ions during sample preparation).

Some of the polycrystalline phases correspond to Ni, and others to WC. Rodelas *et al.* [22] indicated that these crystalline phases are related with the CoxWyCz phases produced in carbon-deficient environments, but additional analysis has to be done. Defects such as dislocations, vacancies, interstitial atoms and stacking faults can be generated at the interface by the solid phase diffusion. Figure 9f) shows a high density of structural defects and the indexation of the inserted SAED pattern indicates a structural disorder along the c axis of the WC structure.

3.3. Diffusion at the interface

The WC-Co/Ni interface is produced by diffusion processes. During the solid phase diffusion bonding process, two metallurgical stages occur concurrently. Firstly, since Ni has less mechanical resistance to compression than WC, the contact area is increased due to the plastic deformation of Ni. This stage lasts few seconds and it is affected by the surface roughness of Ni and WC, surface cleaning, temperature and pressure. The surfaces are brought together and most of the voids or gaps between the two joined surfaces are filled. In the second stage, creep and diffusion are important. The interfacial limit migrates out of the plane of union to the lowest energy equilibrium zone, and the remaining gaps or voids are removed or wrapped.

Therefore, the peaks in the Co and Ni line-scans are produced by diffusion mechanisms, from the region of high concentration to the region of low concentration, as indicated by Fick's Law, and probably due to the accumulation of defects, as commented by Wunderlich [23] who has pointed out the need for dislocations or differences in the thermal expansion

of the metal to obtain the interface. Chen *et al*. [12] indicated that the linear part at the interface, represented by the different slopes in the profile of W, Co, and Ni, is easily adjusted through the diffusion equation. The peaks of Co and Ni profiles can also be interpreted with the diffusion equation in one dimension. The concentration c of each element changes with time following the relationship:

$$\frac{\partial}{\partial x_i}\left(D\frac{\partial}{\partial x_j c}\right) = -\frac{\partial}{\partial t}c + f(r), \tag{1}$$

where D is the diffusion coefficient and $f(r)$ is the source of c in the material. In the stationary case and in the absence of sources, the above expression is reduced to a homogeneous equation:

$$\frac{\partial}{\partial x_i}\left(D\frac{\partial}{\partial x_j c}\right) = 0, \tag{2}$$

whose solution, according to Balluffi *et al*. [24] if D is constant is:

$$c(x) = C(x_1) + cte(x - x_1)\frac{1}{D}. \tag{3}$$

The most interesting part of the concentration behavior at the interface occurs in the non-linear part. The non-linear experimental fact in Co and Ni concentrations (the peaks observed) can be approximated with a Gaussian function. This has two implications. First, the Gaussian profile suggests a change in structure in the region where behavior is no longer linear. Second, the Gaussian profile also suggests that the ratio of the variation with time of concentration is proportional to the concentration at each point. In accordance with the previous correlation analysis, the diffusion equation's behavior inside the rectangles of intensity vs distance shown in Fig. 4 can be considered as:

$$\frac{\partial}{\partial t}c = -\nabla \cdot D\nabla(c) + f(r). \tag{4}$$

Thus, inside the rectangles shown in Fig. 4, c varies in function of time proportionally to the concentration in each point. This is:

$$\frac{\partial}{\partial t}c = (\alpha^2)c, \tag{5}$$

with the constant alpha associated with the element agglomeration. Therefore, with D constant inside the rectangles, the above equation changes to:

$$(D\nabla^2 + \alpha^2)c = f(r), \tag{6}$$

whose solution is the function of Green described by Arfken *et al*. [25]:

$$G(\vec{r} - \vec{r}') = -\frac{1}{4\pi|\vec{r} - \vec{r}'|}\exp(-\alpha|\vec{r} - \vec{r}'|). \tag{7}$$

The fact that a Green function is a solution of the diffusion equation in the Gaussian region gives a physical sense to the experimental concentration graph. The shape of the Green function depends on the alpha value, the parameter of proportionality, which allows to specify the exact shape of the Gaussian function. Therefore, the Green function solution modulates the concentration around the points in the rectangles shown in Fig. 4 where the agglomerations are presented. If alpha is negative, the behavior of the solution is an oscillatory decreasing like a curl. The concentration line scan for W presents a different shape, like a shift in a strip. The diffusion law equation gives a pair of asymmetric equations whose result is a Green function too. The negative value of alpha is transformed into the behavior that explains the other remaining part of W.

4. Conclusions

The analysis of the interface by SEM, TEM and EDS analyses contributes to understand the welding-mechanism for hetero-interface materials. At the interface, diffusion played an important role for the welding between Ni (metal) and WC-Co (cermet). TEM observation of the WC-Co/Ni interface revealed that the solid phase diffusion welding produced an amorphous carbon layer and crystalline phases related to Ni and WC. Electronic affinity, ionization energy, and charge transfer allow diffusion of W into Ni by occupational difference, being the Ni and Co diffusion the most important in the formation of the cermet-metal interface. This diffusion is dominated by a non-linear decay, where the segregation of the element occurs, the concentration follows an exponential decay, suggesting that the punctual variation of concentration goes in a proportional way.

Acknowledgements

Authors would like to thank to CONACYT-México and the Universidad Michoacana de San Nicolás de Hidalgo for the support to develop this work. We appreciate the comments by Drs. A. Rodríguez, E. Salas, B. Campillo and M. Moreno Ríos. The thank Dr. E. M. Saucedo-Salazar and E. Diaz-Barriga of CIQA-Saltillo for helping in the TEM analysis. We also thank S. Tehuacanero Nuñez, S. Tehuacanero Cuapa, P. Lopez Arriaga, C. A. Martínez and A. N. Reyes for technical support. This research did not receive any specific economic grant from funding agencies in the public, commercial, or not-for-profit sectors.

1. L. Ceja-Cárdenas, J. Lemus-Ruiz, S. Dias de la Torre, R. Escalona-González, Interfacial behavior in the brazing of silicon nitride joint using a Nb-foil interlayer. *J Mater. Proc. Tech.* **213** (2013) 411, https://doi.org/10.1016/j.jmatprotec.2012.09.019.
2. M.I. Barrena, J.M. Gómez de Salazar, L. Matesanz, Interfacial microstructure and mechanical strength of WC-Co/90MnCrV8 cold work tool steel diffusion bonded joint with Cu/Ni electroplated interlayer. *Mater. Des.* **31** (2010) 3389, https://doi.org/10.1016/j.matdes.2010.01.050.
3. H.S. Hosseini, M. Shamanian, A. Kermanpur, Microstructural and weldability analysis of Inconel617/AISI 310 stainless steel dissimilar welds. *Int. J. Pres. Ves. Pip.* **144** (2016) 18, https://doi.org/10.1016/j.ijpvp.2016.05.004.
4. K. Martinsen, S.J. Hu, B.E. Carlson, Joining of dissimilar materials. *CIRP Ann-Manuf. Techn.* **64** (2015) 679, https://doi.org/10.1016/j.cirp.2015.05.006.
5. M. Uzkut, N.S. Köksal, B.S. Ünlü, The determination of element diffusion in connecting SAE1040/WC material by brazing. *J. Mater. Proc. Tech.* **169** (2005) 409, https://doi.org/10.1016/j.jmatprotec.2005.05.001.
6. O. Sayman, F. Sen, E. Celik, Y. Arman, Thermal stress analysis of WC-Co/Cr-Ni multilayer coatings on 316L steel substrate during cooling process. *Mater. Des.* **30** (2009) 770, https://doi.org/10.1016/j.matdes.2008.06.004.
7. J. Lemus-Ruiz, L. Ceja-Cárdenas, J.A. Verduzco, O. Flores, Joining of tungsten carbide to nickel by direct diffusion bonding and using a Cu-Zn alloy. *J. Mater. Sci.* **43** (2008) 6296, https://doi.org/10.1007/s10853-008-2894-5.
8. Y. Guo, Y. Wang, B. Gao, Z. Shi, Z. Yuan, Rapid diffusion bonding of WC-Co cemented carbide to 40Cr steel with Ni interlayer: Effect of surface roughness and interlayer thickness. *Cer. Int.* **42** (2016) 16729, https://doi.org/10.1016/j.ceramint.2016.07.145.
9. K. Bonny, P. De Baets, Y. Perez, J. Vleugels, B. Lauwers, Friction and wear characteristics of WC-Co cemented carbides in dry reciprocating sliding contact. *Wear* **268** (2010) 1504, https://doi.org/10.1016/j.wear.2010.02.029.
10. Z. Poniznik, Z. Nowak, M. Batista, Numerical modeling of deformation and fracture of reinforcing fibers in ceramic-metal composites. *Int. J. Dam. Mech.* **26** (2017) 711, https://doi.org/10.1177/1056789515611945.
11. K. Feng, H. Chen, J. Xiong, and Z. Guo, Investigation on diffusion bonding of functionally graded WC.Co/Ni composite and stainless steel. *Mat. Des.* **46** (2013) 622, https://doi.org/10.1016/j.matdes.2012.11.006.
12. H. Chen *et al.*, Characterization and forming process of a functionally graded WC-Co/Ni composite. *Int. J. Refract. Met. Hard Mater*. **35** (2012) 306, https://doi.org/10.1016/j.ijrmhm.2012.04.014.
13. M.N. Avettand-Fénoël, T. Nagaoka, H. Fujii, R. Taillard, Effect of a Ni interlayer on microstructure and mechanical properties of WC-12Co cermet/SC45 steel friction stir welds. *J. Man. Proc.* **40** (2019) 1, https://doi.org/10.1016/j.jmapro.2019.02.032.
14. T. Wagner, R. Kirchheim, M. Rühle, Chemical reactions at metal/ceramic interfaces during diffusion bonding. *Act. Metall. Mater.* **43** (1995) 1053,
15. Z. Zhang, Y. Long, S. Cazottes, R. Daniel, C. Mitterer, G. Dehm, The peculiarity of the metal-ceramic interface. *Sci. Repor.* **5** (2015) 11460, https://doi.org/10.1038/srep11460.
16. A.J. Markworth, K.S. Ramesh, W.P. Parks, Modeling studies applied to functionally graded materials. *J. Mater. Sci.* **30** (1995) 2183, https://doi.org/10.1007/BF01184560.
17. K. Jurkiewicz, M. Pawlyta, A. Burian, Structure of carbon materials explored by local transmission electron microscopy and global powder diffraction probes. *J. Carbon Res.* **4** (2018) 68, https://doi.org/10.3390/c4040068.
18. J. Reyes-Gasga, M. Jose-Yacaman, Quasicrystalline phases and rational approximants obtained from vapor deposited Al Mn thin films. *J. Vac. Sci. Tech. A* **8** (1990) 3455, https://doi.org/10.1116/1.576531.
19. J. Reyes-Gasga, G. Mondragón-Galicia, and M. Jose-Yacaman, Insitu TEM observation of phase transitions in thin films of the Al-Mn system. *Thin Sol. Films* **227** (1993) 24, https://doi.org/10.1016/0040-6090(93)90182-0.
20. J. Reyes-Gasga, R. Garcia, Opening and closing of channels during phase transitions in Al-Mn thin films. *Thin Sol. Films* **253** (1994) 254, https://doi.org/10.1016/0040-6090(94)90330-1.
21. J. Reyes-Gasga, R. Garcia, L. Vargas-Ulloa, In-situ observation of fractal structures and electrical conductivity in human tooth enamel. *Phil. Magaz. A* **75** (1997) 1023, https://doi.org/10.1080/01418619708214008.
22. J. Rodelas, G. Hilmas, R.S. Mishra, Sintering cobalt-cemented tungsten carbide to tungsten heavy alloys. *Int. J. Refract. Met. Hard Mater.* **27** (2009) 835, https://doi.org/10.1016/j.ijrmhm.2009.03.001.
23. W. Wunderlich, The atomistic structure of metal/ceramic interfaces is the key issue for developing better properties. *Met.* **4** (2014) 410, https://doi.org/10.3390/met4030410.
24. R. W. Balluffi, S. M. Allen, and W. C. Carter, Kinetics of Materials, in R.A. Kemper (Ed.), (Willey Interscience, John Wiley and Sons, Inc. Publication, USA, 2005).
25. G.B. Arfken, H.J. Weber, F.E. Harris, Mathematical Methods for Physicists: A Comprehensive Guide, 7th ed. (Academic Press, 2012), Table 9.5.